Acta Crystallographica Section D
Biological Crystallography
ISSN 0907-4449

High-resolution structure of exo-arabinanase from *Penicillium chrysogenum*

Yuri Sogabe,[a] Tomoya Kitatani,[b] Asako Yamaguchi,[a] Takayoshi Kinoshita,[a] Hiroaki Adachi,[c,d,e] Kazufumi Takano,[c,d,e] Tsuyoshi Inoue,[c,d,e] Yusuke Mori,[c,d,e] Hiroyoshi Matsumura,[c,d,e] Tatsuji Sakamoto[b] and Toshiji Tada[a]*

[a]Graduate School of Science, Osaka Prefecture University, Sakai, Osaka 599-8531, Japan, [b]Graduate School of Life and Environmental Sciences, Osaka Prefecture University, Sakai, Osaka 599-8531, Japan, [c]Graduate School of Engineering, Osaka University, Suita, Osaka 565-0871, Japan, [d]SOSHO Inc., Osaka 541-0053, Japan, and [e]CREST, JST, Suita, Osaka 565-0871, Japan

Correspondence e-mail: tada@b.s.osakafu-u.ac.jp

Received 19 November 2010
Accepted 19 February 2011

PDB References: Abnx, 3a71; complex with arabinobiose, 3a72.

Arabinanase Abnx from *Penicillium chrysogenum* 31B, which belongs to the GH93 family, releases arabinobiose from the nonreducing terminus of α-1,5-L-arabinan, which is distributed in the primary cell walls of higher plants. Crystal structures of Abnx and of its complex with arabinobiose were determined at the high resolutions of 1.14 Å to an R_{work} of 10.7% (R_{free} = 12.8%) and 1.04 Å to an R_{work} of 10.4% (R_{free} = 12.5%). Abnx has a six-bladed β-propeller fold with a typical ring-closure mode called 'Velcro', in which the last four-stranded β-sheet is completed by the incorporation of a strand from the N-terminus. Catalytic residues which act as a nucleophile and an acid/base were proposed from the structures and confirmed by site-directed mutagenesis. The substrate-binding groove is enclosed at one end by two residues, Glu64 and Tyr66, which contribute to the recognition of the nonreducing chain end of the polysaccharide. A comparison with the related enzyme Arb93A which has a quite similar overall structure suggested that Abnx has different mechanisms to funnel substrates to the active site and/or to stabilize the transition state.

1. Introduction

Arabinans are distributed in pectins, which occur in the matrix of the primary cell walls of higher plants. The neutral polysaccharides of pectins have been reported to play important roles in plant cell development (Willats *et al.*, 1999) and in maintaining flexibility in the cell wall (Jones *et al.*, 2003). The backbone of arabinan consists of α-1,5-linked arabinofuranosyl units branched with α-1,2- or α-1,3-linked side chains of arabinose in the furanose conformation (Bacic *et al.*, 1988). Arabinan-degrading enzymes are classified by their substrate specificity. α-L-Arabinanases (EC 3.2.1.–) hydrolyze α-L-arabinofuranoside linkages and α-L-arabinofuranosidases (EC 3.2.1.55) cleave arabinose side chains. They act synergistically to reduce arabinan to arabinose and/or arabinooligosaccharides (Kaneko *et al.*, 1998). These enzymes have become of interest in recent years because of their potential application in various industrial processes: the improvement of wine flavours, juice clarification, the production of non-calorific sweeteners and the production of bioethanol (Seri *et al.*, 1996; Numan & Bhosle, 2006).

Based on amino-acid sequence similarity, the α-L-arabinanases have been classified into two glycoside hydrolase (GH) families: 43 and 93 (Henrissat, 1996; Cantarel *et al.*, 2009). GH93 enzymes hydrolyze the glycosidic linkages with

net retention of configuration at the anomeric C atom, whereas GH43 enzymes act with an inverting mechanism. Currently, four crystal structures of GH43 α-L-arabinanases, including an exo-type arabinanase (Nurizzo *et al.*, 2002) and three endo-type arabinanases (Yamaguchi *et al.*, 2005; Proctor *et al.*, 2005; Alhassid *et al.*, 2009), have been reported. All of these enzymes have a common unique motif of a five-bladed β-propeller fold consisting of five β-sheets, each of which is made up four β-strands in an antiparallel arrangement. Recently, the three-dimensional structure of an exo-type arabinanase, Arb93A, belonging to the GH93 family was elucidated to contain a unique six-bladed β-propeller fold by X-ray crystallography at 1.85 Å resolution (Carapito *et al.*, 2009). The inverting GH43 arabinanase adopts the five-bladed β-propeller fold, whereas interestingly the retaining GH93 arabinanase adopts the six-bladed β-propeller fold.

A new exo-α-L-arabinanase, Abnx, was isolated from a culture filtrate of *Penicillium chrysogenum* 31B (Sakamoto & Thibault, 2001) and was classified into the GH93 family (Sakamoto, 2006). The Abnx gene codes for a 378-amino-acid protein containing a signal peptide and a propeptide. The mature Abnx is composed of 355 amino acids with a molecular weight of 40 kDa. The enzyme releases arabinobiose from the nonreducing terminus of α-1,5-L-arabinan without inverting the anomeric configuration and shows no activity towards arabinobiose (Sakamoto, Ihara *et al.*, 2004; Sakamoto, Fujita *et al.*, 2004). The kinetic parameters of Abnx differ from those of Arb93A towards arabino-oligosaccharides with degrees of polymerization (DPs) from three to six.

Here, we report the crystal structures of native Abnx and its complex with arabinobiose (DP2) at 1.14 and 1.04 Å resolution, respectively. A detailed study of the three-dimensional structure of the enzyme at high resolution, comparing it with that of Arb93A, should provide some information regarding the recognition mechanism for arabino-oligosaccharides. The elucidation of the substrate-recognition mechanisms of the arabinan-degrading enzymes will enable understanding of the structure of plant cell walls, which constitute the most diverse group of polysaccharides.

2. Materials and methods

2.1. Protein cloning, expression and purification

Recombinant Abnx of *P. chrysogenum* was overexpressed in *Escherichia coli*. The DNA fragments encoding the mature form consisting of residues 24–378 were amplified by PCR using the primers 5′-ATA**CATCTG**TCTTCTCCTACCTCGC-TCACA-3′ and 5′-CGC**GGATCC**TTACAATACTTCTTTC-AAGT-3′ with *Nde*I and *Bam*HI restriction sites (bold). The PCR product was ligated to the TA cloning vector pT7 Blue (TAKARA). The pT7 Blue-*Abnx* plasmid was digested and the resulting Abnx gene was inserted into the pET3a expression vector (Novagen). Competent *E. coli* BL21 (DE3) pLysS cells transformed by pET3a-Abnx were cultured in Luria–Bertani broth (LB) supplemented with 100 μg ml^{-1} ampicillin, 34 μg ml^{-1} chloramphenicol and 0.2%(*w*/*v*) glucose at 310 K. Protein expression was induced by addition of 1 m*M* isopropyl β-D-1-thiogalactopyranoside (IPTG) at an $A_{600\,\mathrm{nm}}$ of 0.5 and cultivation was continued for a further 5.5 h at 310 K. The cells were harvested, resuspended in 50 m*M* phosphate buffer pH 7.0 (buffer *A*) and sonicated. The supernatant containing soluble Abnx was separated from the pellet by centrifugation.

The concentrated supernatant was loaded onto a HiPrep 16/10 DEAE column (GE Healthcare Life Sciences) equilibrated with buffer *A* and eluted with a linear gradient of NaCl (0–0.4 *M*) on an ÄKTA FPLC system (GE Healthcare Life Sciences). The active fractions were combined and adjusted to 20%(*w*/*v*) ammonium sulfate. After centrifugation, the supernatant was loaded onto a HiPrep 16/10 Butyl FF column (GE Healthcare Life Sciences) equilibrated with buffer *A* containing 20%(*w*/*v*) ammonium sulfate and eluted with a linear gradient of ammonium sulfate [20–0%(*w*/*v*)] in buffer *A*. The recombinant Abnx was finally purified by gel-filtration chromatography using a Superdex-75 10/300 GL column (GE Healthcare Life Sciences) in buffer *A* containing 0.1 *M* NaCl. The resulting active fractions were concentrated using an ultrafiltration membrane (Millipore) with a molecular-weight cutoff (MWCO) of 10 kDa and the purity was confirmed by SDS–PAGE.

The selenomethionine-substituted (SeMet) derivative was expressed in the *E. coli met*$^{-}$ auxotrophic strain B834 (DE3) pLysS. The transformed cells were grown in 5 ml LB medium followed by overnight incubation at 310 K. The 5 ml preculture was inoculated into 1 l M9 medium supplemented with 10 μg ml^{-1} ampicillin, 34 μg ml^{-1} chloramphenicol, 0.1%(*v*/*v*) vitamin cocktail (Kao and Michaylik Vitamin Solution, Sigma), 0.5%(*w*/*v*) glucose and 30 μg ml^{-1} seleno-L-methionine (Sigma). The medium was incubated at 310 K to an $A_{600\,\mathrm{nm}}$ of 0.8 and immediately cooled to 291 K. Protein expression was induced by the addition of 1 m*M* IPTG. After cultivation for 48 h, the cells were harvested, resuspended in buffer *A* and sonicated. SeMet-labelled Abnx was purified with the same chromatographic techniques as were used in the purification of wild-type Abnx. The purity was confirmed by SDS–PAGE.

Site-directed mutagenesis of Abnx was carried out using the QuikChange kit (Stratagene). The sequences of the mutant were verified by DNA sequencing with a dye-terminator cycle sequencing kit (Beckman Coulter) and a CEQ2000 fragment-analysis system (Beckman Coulter).

2.2. Enzyme assay

The enzymatic activity was assayed by the Somogyi–Nelson method (Nelson, 1944; Somogyi, 1952) measuring the amount of reducing sugars formed in a mixture comprising 200 μl 0.5%(*w*/*v*) sugar beet debranched α-1,5-L-arabinan (Megazyme International) as a substrate in 100 m*M* acetate buffer pH 5.0 and 10 μl of an appropriately diluted enzyme solution with incubation at 310 K for 30 min. One unit of arabinanase activity was defined as the amount of enzyme required to

produce 1 m*M* of reducing sugar equivalent to arabinobiose per minute under the assay conditions.

2.3. Crystallization and data collection

Crystallization conditions were screened by the sitting-drop vapour-diffusion method using 5 mg ml^{-1} protein in 50 m*M* HEPES buffer pH 7.0 and the commercially available Wizard I and II sparse-matrix screening kits (Emerald BioSystems) at 277 K. Small crystals were obtained from formulation No. 9 of Wizard II containing 2.0 *M* ammonium sulfate as a precipitant. Crystals were grown in the form of cubes with dimensions of approximately 0.3 mm by the macroseeding method, in which a small crystal was transferred to a fresh drop of Abnx solution pre-equilibrated to the growth conditions overnight (Fig. 1*a*). The growth conditions involved mixing 1 µl 8 mg ml^{-1} Abnx in 50 m*M* phosphate buffer pH 7.0 with the same volume of reservoir solution consisting of 1.8 m*M* ammonium sulfate and 100 m*M* sodium citrate buffer pH 2.7. The crystals were determined to belong to the tetragonal space group $P4_122$ (or its enantiomorph $P4_322$) based on the symmetry and the systematic absences of the reflections, with unit-cell parameters $a = b = 166.9$, $c = 401.5$ Å. Assuming 16–8 molecules of Abnx in the asymmetric unit, the V_M value was calculated to be 2.2–4.4 Å^3 Da^{-1}, corresponding to a solvent content of 44–72%.

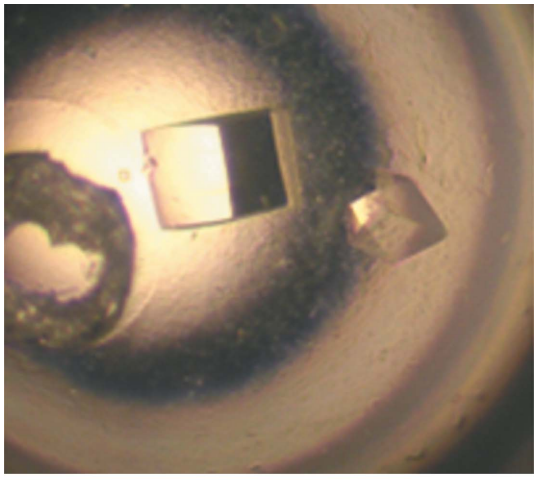

(*a*)

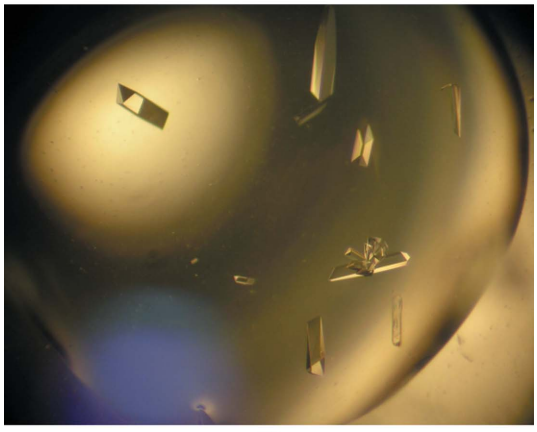

(*b*)

Figure 1
Typical crystals of exo-α-L-arabinanase Abnx from *P. chrysogenum*. The dimensions of the tetragonal crystals (*a*) and the octahedral crystals (*b*) were approximately 0.3 × 0.3 × 0.3 and 0.3 × 0.1 × 0.1 mm, respectively.

Since high-resolution data collection was difficult using the tetragonal crystals, we sought new crystal forms by using the laser-irradiated growth technique (LIGHT) in combination with a solution-stirring technique, called COLAS, provided by SOSHO Inc. (Adachi, Takano, Hosokawa *et al.*, 2003; Adachi, Takano, Yoshimura *et al.*, 2003; Adachi *et al.*, 2005). The protein and reservoir solutions were mixed in a 1:1 ratio and a 6 µl aliquot was used for the crystallization drop. The drop was sealed in a specially designed crystallization plate (Cybox) that holds a proportionally larger volume of reservoir solution. A short-pulse laser beam irradiated the drop through the bottom of the plate. A femtosecond laser system (Continuum) was used to provide 200 fs pulses at a repetition rate of 1 kHz and a wavelength of 780 nm. The crystals were grown by the microstirring technique using a rotary shaker with a rotation speed of 50 rev min^{-1} and a swing amplitude of 40 mm. This technique is expected to enhance the probability of protein crystallization because it promotes nucleation. As a result, a new crystal belonging to the orthorhombic crystal system was obtained under crystallization conditions containing 2-methyl-2,4-pentanediol (MPD) as a precipitant. After optimization of the conditions, orthorhombic crystals grew to maximum dimensions of 0.5 × 0.1 × 0.08 mm in four weeks using the hanging-drop vapour-diffusion method (Fig. 1*b*). A drop was prepared by mixing 1 µl 5.5 mg ml^{-1} Abnx in 50 m*M* HEPES buffer pH 7.0 with 1 µl reservoir solution consisting of 28%(*v*/*v*) MPD and 100 m*M* sodium acetate buffer pH 4.5 and was equilibrated against 1 ml reservoir solution. A diffraction data set was collected from the native crystal on an ADSC CCD detector using synchrotron radiation of wavelength 0.90 Å at the BL41XU station of SPring-8, Japan. The crystal-to-detector distance was 150 mm and the oscillation range was 1° per image. For data collection at 100 K, the crystal was loop-mounted in a cryoprotectant solution consisting of 34%(*v*/*v*) MPD and 100 m*M* acetate buffer pH 4.5. The crystal diffracted to 1.14 Å resolution. The crystal belonged to the orthorhombic space group $P2_12_12_1$, with unit-cell parameters $a = 66.88$, $b = 77.25$, $c = 79.44$ Å. Assuming the presence of one molecule of Abnx in the asymmetric unit, the V_M value was calculated to be 2.6 Å^3 Da^{-1}, corresponding to a solvent content of 52.7%.

Crystals of Abnx complexed with arabinobiose (DP2) were prepared by a soaking method using a large excess of DP2. Complete X-ray diffraction data were collected on an ADSC CCD detector using synchrotron radiation of wavelength 1.00 Å at 100 K at the NW12 station of PF-AR, Japan. The crystal diffracted to 1.04 Å resolution.

The crystallization of SeMet-labelled Abnx was carried out using 26%(*v*/*v*) MPD and 100 m*M* acetate buffer pH 4.0 as a reservoir solution. Multiple-wavelength anomalous diffraction (MAD) data were collected at the absorption peak (λ = 0.9792 Å), inflection point (λ = 0.9794 Å) and a high-energy remote point (λ = 0.9700 Å) with a crystal-to-detector distance of 200 mm at the BL41XU station of SPring-8, Japan.

Table 1
Summary of data-collection and refinement statistics.

Values in parentheses are for the highest resolution shell.

		Selenomethionine			
Data set	Native	Peak	Edge	Remote	Arabinobiose complex
Data-collection statistics					
X-ray source	BL41XU, SPring-8	BL41XU, SPring-8			NW12, PF-AR
Wavelength (Å)	0.9	0.9792	0.9794	0.9700	1.0
Temperature (K)	100	100			100
Space group	$P2_12_12_1$	$P2_12_12_1$			$P2_12_12_1$
Unit-cell parameters (Å)	a = 66.88, b = 77.25, c = 79.44	a = 65.91, b = 76.69, c = 79.03			a = 66.96, b = 77.12, c = 79.57
Resolution (Å)	50–1.14 (1.18–1.14)	50–1.60 (1.66–1.60)			50–1.04 (1.08–1.04)
Average $I/\sigma(I)$	32.0 (2.4)	22.6 (1.7)	22.2 (1.7)	25.1 (1.7)	26.5 (2.3)
No. of observed reflections	1069416	385830	384185	390807	1378364
No. of unique reflections	141611	53407	53330	53515	186439
$R_{\rm merge}$†	11.3 (34.2)	11.8 (37.4)	9.1 (39.9)	9.4 (34.3)	5.3 (36.3)
Completeness (%)	99.7 (99.0)	97.6 (95.3)	97.6 (95.4)	97.8 (95.3)	99.6 (98.0)
Refinement statistics					
Resolution limits (Å)	19.86–1.14				19.75–1.04
$R_{\rm work}$‡/$R_{\rm free}$§	10.7/12.8				10.4/12.5
R.m.s.d. bond lengths (Å)	0.016				0.017
R.m.s.d. angles (°)	2.1				2.0
No. of atoms					
Protein	2771				2771
Ligand					19
Solvent	24				
Ions	4				
Water	542				546
B factors (Å^2)					
Protein	8.4				7.9
Ligand					4.9
Solvent	5.4				
Ions	7.1				
Water	22.7				22.7

† $R_{\rm merge} = \sum_{hkl}\sum_i |I_i(hkl) - \langle I(hkl)\rangle| / \sum_{hkl}\sum_i I_i(hkl)$. ‡ $R_{\rm work} = \sum_{hkl} \big||F_{\rm obs}| - |F_{\rm calc}|\big| / \sum_{hkl} |F_{\rm obs}|$. § $R_{\rm free}$ was calculated using 5% of the data.

Data collection was performed using an SeMet-labelled Abnx crystal at 100 K. All data sets were processed and scaled using the *HKL*-2000 software package (Otwinowski & Minor, 1997). Data-collection statistics are summarized in Table 1.

2.4. Phasing, model building and refinement

Initial phases were determined by the MAD method using Se with the program *SOLVE* (Terwilliger & Berendzen, 1999). Three of the four Se atoms in the asymmetric unit were identified, giving an overall figure of merit of 0.63. The initial phases were improved by density modification using the program *RESOLVE* (Terwilliger, 2000) with a solvent content of 52.4%, resulting in an overall figure of merit of 0.77. Using the phase information, initial model building was performed automatically with the program *ARP*/*wARP* (Morris *et al.*, 2002). The initial model consisted of 349 amino-acid residues (∼98%). Visual modifications of the models and crystallographic refinement were carried out using the programs *XtalView* (McRee, 1999) and *REFMAC*5 (Winn *et al.*, 2003). The structure of SeMet-labelled Abnx including 353 amino-acid residues was characterized by an $R_{\rm work}$ of 24.1% and an $R_{\rm free}$ of 26.4%. For $R_{\rm free}$ calculations, 2667 (5%) reflections were randomly selected from the full resolution range 20.0–1.60 Å.

The coordinates of the isomorphous SeMet-labelled Abnx were used for initial phasing of wild-type Abnx. The initial model was refined by several cycles of rigid-body positioning with B-factor optimization. The resultant $R_{\rm work}$ and $R_{\rm free}$ were 26.5% and 26.7%, respectively. The quality of the model was gradually improved by alternating rounds of refinement with *REFMAC*5 and model building with *XtalView* until the $R_{\rm work}$ and $R_{\rm free}$ values dropped to 24.6% and 25.0%, respectively. The $F_{\rm o} - F_{\rm c}$ difference map showed electron densities which were suggestive of three MPD molecules and an acetate ion. After several rounds of refinement including the MPD molecules and acetate ion, water molecules were added to the model at locations with $F_{\rm o} - F_{\rm c}$ densities higher than 3.0σ and hydrogen-bonding stereochemistry using the water-pick function of *ARP*/*wARP*. The isotropic refinement converged to $R_{\rm work}$ and $R_{\rm free}$ values of 14.4% and 16.0%, respectively. The structure was further refined using *SHELXL* (Sheldrick, 2008) in conjugate-gradient least-squares (CGLS) mode against F^2. After the first three rounds of isotropic refinement, the non-H atoms were refined anisotropically in all subsequent refinement cycles. The first round of anisotropic refinement resulted in a sharp decrease of $R_{\rm work}$ to 11.6% and of $R_{\rm free}$ to 14.3%. H atoms were added to the model according to geometrical criteria implemented in *SHELXL*. This yielded a decrease of 0.9% in $R_{\rm work}$ and of 1.3% in $R_{\rm free}$ without increasing the number of parameters. Water molecules with B factors higher than 60 Å^2 were deleted from subsequent refinement rounds. The final crystallographic refinement converged with $R_{\rm work}$ and $R_{\rm free}$ values of 10.7% and 12.8%, respectively.

Refinement of the structure of Abnx complexed with DP2 started with the coordinates of wild-type Abnx. All solvent atoms were removed from the starting model. After several rounds of refinement using *REFMAC*5, $R_{\rm work}$ and $R_{\rm free}$ were reduced to 26.7% and 27.0%, respectively. The $F_{\rm o} - F_{\rm c}$ difference map showed clear electron density corresponding to the DP2 molecule, which adopted an α-configuration of the anomeric C atom, in a deep L-shaped groove. After refinement including the DP2 molecule, water molecules were added to the model using the water-pick function of *ARP*/*wARP*. The isotropic refinement converged with $R_{\rm work}$ and $R_{\rm free}$ values of 14.7% and 15.7%, respectively. The structure

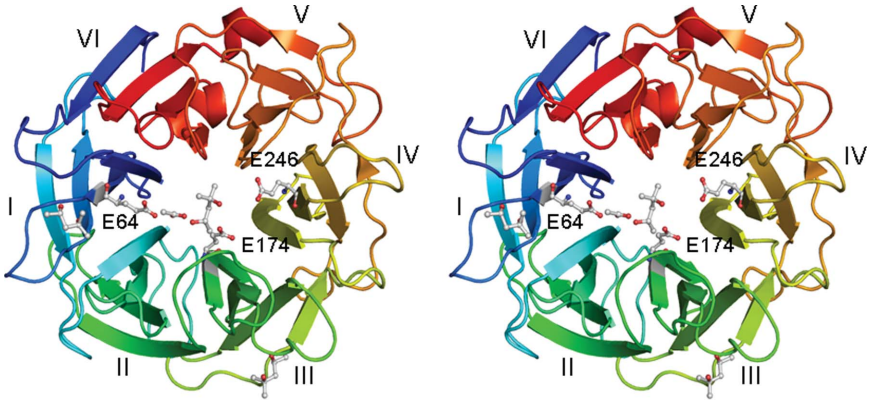

Figure 2
Stereoview of Abnx shown as a ribbon diagram. Each blade is shown in a different colour. Three acidic residues, Glu64, Glu174 and Glu246, three MPD molecules and an acetate ion are shown as ball-and-stick models.

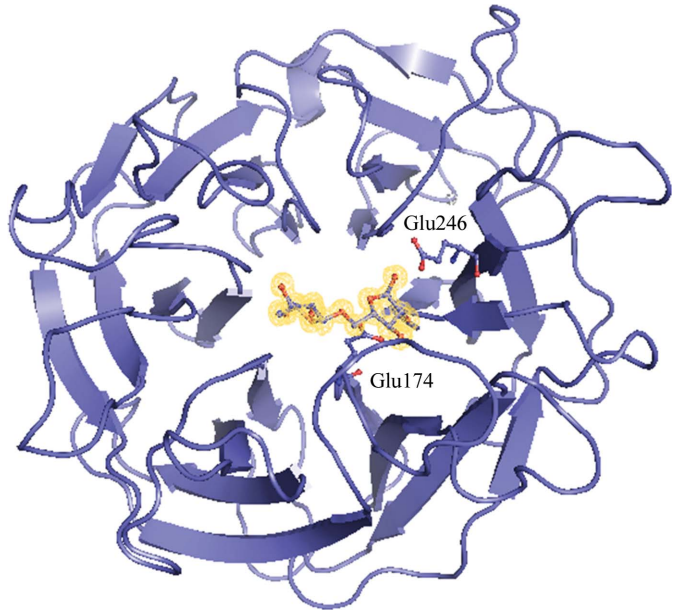

Figure 3
Overall structure of Abnx in complex with arabinobiose. $F_o - F_c$ electron density contoured at the 3σ level at the substrate-binding site is shown in orange. The catalytic residues, Glu174 and Glu246, are shown as ball-and-stick models.

was further refined anisotropically using *SHELXL* against F^2. The resultant R_{work} and R_{free} were 11.8% and 13.9%, respectively. The final crystallographic refinement including H atoms converged with R_{work} and R_{free} values of 10.4% and 12.5%, respectively.

The refinement statistics are given in Table 1. The quality of the models was checked with *PROCHECK* (Laskowski *et al.*, 1993); two amino-acid residues, Arg45 and Ser289, fell in the disallowed region of the Ramachandran plot in both structures. The coordinates and X-ray data have been submitted to the Protein Data Bank with accession codes 3a71 and 3a72. Illustrations were prepared using the *PyMOL* molecular-graphics system (DeLano, 2002).

3. Results and discussion

3.1. Overall structure of Abnx

The crystallization conditions of Abnx have been successfully established using a novel technique referred to as COLAS, in which LIGHT and solution-stirring techniques are applied simultaneously. High-quality crystals of Abnx could be obtained using a high concentration of MPD as a precipitant even when these techniques were not applied; however, around one month was necessary for crystal growth and crystals were not formed in all drops.

The crystal structure of Abnx was solved by MAD using an SeMet derivative. The final model determined at a high resolution of 1.14 Å is comprised of an Abnx molecule, three MPD molecules, an acetate ion and 542 water molecules in the asymmetric unit. The structure of Abnx is shown in Fig. 2. Two amino-acid residues from the N-termini were disordered and did not show clear electron density for assignment. Abnx has a β-propeller fold consisting of six β-sheets, called blades, which are radially arranged around the pseudo-sixfold axis. Each blade is made up of four β-strands in an antiparallel arrangement. A large cavity is elongated along the pseudo-sixfold axis and is filled with water molecules to form a continuous column of water. The structure has a prominent groove, the substrate-binding site, which traverses one face of the propeller. One acetate ion and one MPD molecule were found in the substrate-binding site. The O atom of an acetate ion or acetic acid forms a hydrogen bond to the $O^{\varepsilon 1}$ atom of Glu64 with a distance of 2.5 Å, suggesting the formation of a low-barrier hydrogen bond (Cleland & Kreevoy, 1994; Schiøtt *et al.*, 1998). The MPD molecule is located between amino-acid residues Pro165 and Tyr337 and is linked by a hydrogen bond to the acetate ion/acetic acid. The other two MPD molecules are located around the first and third blades, respectively. One of the two MPD molecules is linked to Ile20 of the first blade by hydrogen bonds *via* a water molecule and the other is linked to Asp190 of the third blade by a direct hydrogen bond.

One of the remarkable features of the β-propeller fold is that the N- and C-termini are linked to form a closed circle (Fülöp & Jones, 1999). Abnx has a typical ring-closure mode called 'Velcro' in which the last four-stranded β-sheet is completed by the incorporation of a strand from the N-terminus. This ring-closure mode contributes to the stability of the circular β-propeller fold, with hydrophobic interactions between neighbouring blades (Jawad & Paoli, 2002).

3.2. Substrate-binding site and catalytic residues

To clarify the substrate-binding site and catalytic residues, a 1.04 Å resolution structure of Abnx complexed with arabinobiose (DP2) was determined (Figs. 3 and 4). The overall structure of Abnx in the complex was almost identical to that of wild-type Abnx, as indicated by the r.m.s.d. value of

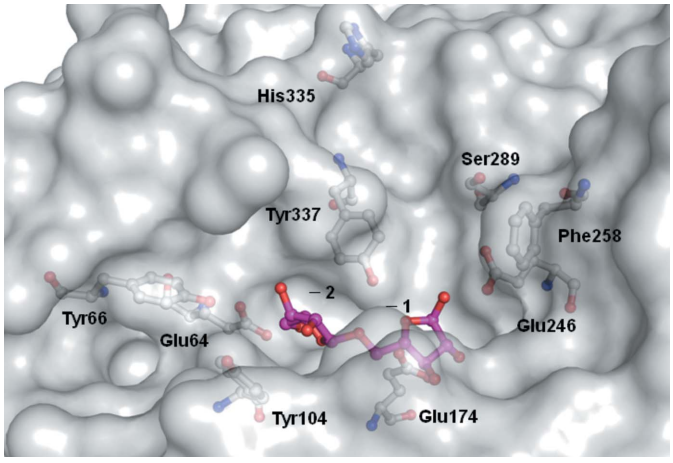

Figure 4
Surface representation of the substrate-binding site (L-shaped groove) of Abnx in complex with arabinobiose. Arabinobiose and amino-acid residues surrounding substrate-binding sites are shown as ball-and-stick models.

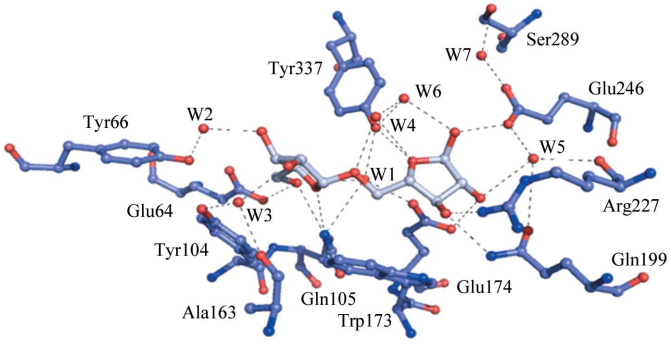

Figure 5
A diagram of the interactions among amino-acid residues of Abnx, water molecules and arabinobiose. Water molecules (W1–W7) are shown as spheres. Potential hydrogen bonds are shown as dotted lines.

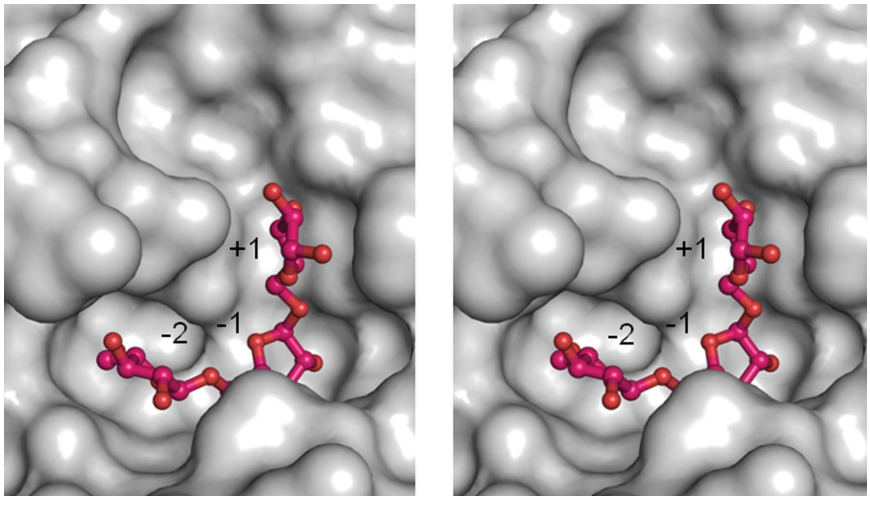

Figure 6
Stereoview showing the surface of the substrate-binding site (L-shaped groove) of Abnx. Arabinotriose is shown as a ball-and-stick model.

0.08 Å for the C^{α} atoms. The subsites occupied by the arabinofuranoside moieties of DP2 were identified as −2 and −1. DP2 binds to the active site of the enzyme through hydrogen bonds and hydrophobic interactions (Fig. 5). Abnx is an exo-type arabinan-degrading enzyme and releases α-1,5-L-arabinobiose from the nonreducing terminus of α-1,5-L-arabinan with retention of the anomeric configuration (Sakamoto *et al.*, 2004). In the −2 subsite the O5 hydroxyl group of the arabinofuranoside moiety forms a hydrogen bond to Glu64 $O^{\delta2}$ (2.7 Å), contributing to the specific recognition of the nonreducing end of α-1,5-L-arabinan. As shown in Fig. 4, the −2 subsite seems to be blocked by the bulky residue Tyr66. Thus, this residue can be considered to contribute to the exo mode of action. The other hydroxyl groups, O2 and O3, of the arabinofuranoside moiety in the −2 subsite interact with Tyr104 OH, the Ala163 carbonyl O atom and Tyr66 OH through hydrogen bonds mediated by water molecules.

The retaining glycosidase cleaves the glycosidic bond using two carboxylic acids that act as a nucleophile and an acid/base. The carboxyl O atom of Glu174 is at an appropriate distance (3.1 Å) for nucleophilic attack on the anomeric carbon C1 of the arabinofuranoside moiety occupying the the −1 subsite. The carboxyl O atom of Glu246 is located 2.6 Å from the glycosidic oxygen O1 of the moiety at the −1 subsite, allowing the required acid catalysis and the direct protonation of the departing aglycone. Each of the two residues Glu246 and Glu174 was mutated to alanine and glutamine and the activities of the resulting mutants, Abnx-E246A/Q and Abnx-E174A/Q, were compared with that of the wild-type Abnx. As expected, all four mutants did not show enzyme activity using debranched arabinan as a substrate with incubation at 310 K for 30 min. The arabinofuranoside moiety in the −1 subsite binds tightly to Abnx by hydrogen bonds. The O2 and O3 hydroxyl groups of the arabinofuranoside moiety form hydrogen bonds to Glu174 $O^{\delta1}$ (2.9 Å) and Arg229 $N^{\zeta2}$ (3.0 Å), respectively. The O4 ring O atom forms a hydrogen bond to Tyr337 OH (3.2 Å). Thus, it can be considered that the substrate binds tightly to Abnx in the −1 subsite and that the −1 subsite plays a critical role in the substrate recognition of Abnx.

Kinetic parameters of the recombinant MBP-fusion Abnx towards arabino-oligosaccharides with different DPs (DP3 to DP7) have been reported by Sakamoto (2006). k_{cat}/K_m increased with an increase in the DP (DP3 to DP6), reaching the highest value at DP6. K_m decreased with an increase in the DP (DP3 to DP6), reaching the lowest value at DP6. This indicates that Abnx has at least six subsites. The shape of the active-site groove and the position of the hydroxyl group O1 atom of DP2 seem to indicate that the +1 subsite is located in a basin surrounded by four amino-acid residues: Glu246, Phe258, Ser289 and Tyr337 (Figs. 4 and 6). The third arabinofuranoside moiety

was constructed using *Discovery Studio* (Accelrys) referring to the positions of the water molecules (Fig. 6). The moiety in the +1 subsite is sandwiched from both sides by amino-acid residues Tyr337 and Phe258. It is indicated that the O4 hydroxyl group of the moiety forms a hydrogen bond to Glu246 $O^{\delta1}$ (3.1 Å). The polysaccharide chain which is accommodated in the active site will be bent ∼90° between the −1 and +1 subsites. After the +1 subsite, the substrate-binding groove seems to extend toward His335 (Figs. 4 and 6).

3.3. Comparison with arabinanase belonging to GH93 family

The overall structure of Abnx is quite similar to that of Arb93A, which has 53% homology to Abnx, as indicated by the low r.m.s.d. value of 0.9 Å for the C^{α} atoms. The binding mode of DP2 is also similar to that found in the structure of Arb93A complexed with DP2 (Carapito *et al.*, 2009). However, the activity of Abnx is only a thousandth of that of Arb93A towards arabinotetraose (DP4), arabinopentaose (DP5) and arabinohexaose (DP6). The k_{cat}/K_m values of Abnx range from 1.15×10^4 to 3.92×10^4 s^{-1} M^{-1} (Sakamoto, 2006) and those of Arb93A range from 1.05×10^7 to 4.66×10^7 s^{-1} M^{-1} (Carapito *et al.*, 2009). The k_{cat}/K_m values of Arb93A indicate that Arb93A molecules catalyze a reaction almost every time they encounter a substrate molecule. On the other hand, in Abnx many substrate molecules seem to leave the active site without catalytic reaction. In other words, Abnx has some substrate-binding modes that are difficult to shift to a transition state.

A notable sequence difference between Abnx and Arb93A has been found in the substrate-binding site. Abnx contains Ser289 in the +1 subsite, whereas Arb93A contains Gly288. Compared with Arb93A, the groove of the +1 subsite of Abnx is somewhat narrow and shallow. Moreover, the hydroxyl group of Ser289 has the potential to form a hydrogen bond to the hydroxyl group, especially O3, of the arabinofuranoside moiety which is located in the +1 subsite. Thus, the arabinofuranoside moiety bound in the +1 subsite of Abnx may have a different orientation from that in Arb93A. A significant difference is also found in the location of the arabinofuranoside moiety in the −1 subsite between Abnx and Arb93A. In the present Abnx–DP2 complex structure the distances from the hydroxyl group O1 and anomeric carbon C1 of the arabinofuranoside moiety to Tyr337 OH are 4.2 and 3.9 Å, respectively. In contrast, the Arb93A–DP2 complex structure has shorter distances of 3.4 and 3.5 Å, respectively. The mutant Abnx-Y337A retained 50% of the activity of the wild-type, whereas the activity of the mutant Arb93A-Y337A was reported to decrease to 7% (Carapito *et al.*, 2009). These results suggest that Abnx has different mechanisms to funnel substrates to the active site and/or to stabilize the transition state.

It is worth noting that Arb93A has Arg38 in the equivalent position to Ile20 of Abnx. The isoleucine residue has a small side chain compared with the arginine residue. Thus, a cavity is generated around Ile20 of Abnx. In the native crystal of Abnx one MPD molecule is found in the cavity. In the complex structure, however, an MPD molecule could not be found in the cavity, even though 28%(*v*/*v*) MPD was included in the crystallization conditions. A large excess of DP2 seems to interfere with MPD binding in the cavity. It might be assumed that the arabinofuranoside moiety can bind to the same site as MPD, although electron density corresponding to the DP2 molecule cannot clearly be found in the cavity. As shown in Fig. 4, the cavity is a part of a shallow ditch connected to the deep L-shaped groove including the −2 and −1 subsites. Thus, the polysaccharide chain, which binds to the shallow ditch, is not only hydrolyzed but also has potential to act as an inhibitor. Such substrate binding does not seem to occur in Arb93A because it does not have a cavity at the same position. Thus, it can be concluded that the Ile20 residue suppresses the enzymatic function of Abnx.

4. Conclusions

We have determined the crystal structures of the exo-α-1,5-L-arabinanase Abnx from *P. chrysogenum* 31B by MAD using the SeMet derivative and of its complex with arabinobiose at high resolutions of 1.14 and 1.04 Å, respectively. The crystallization conditions giving high-quality crystals of Abnx were successfully established by the novel technique referred to as COLAS. Abnx has a β-propeller fold consisting of six β-sheets, each of which is made up of four β-strands in an antiparallel arrangement. The structures and site-directed mutagenesis proposed Glu174 and Glu246 as the catalytic residues, acting as a nucleophile and an acid/base, respectively. A striking feature of Abnx is a prominent groove, the substrate-binding site, that is enclosed at one end by two residues, Glu64 and Tyr66, and contributes to the recognition of the nonreducing chain end of the polysaccharide. The structures presented here could reveal that Abnx has different mechanisms to funnel substrates to the active site and/or to stabilize the transition state compared with the related arabinan-degrading enzyme Arb93A, which has a quite similar structure and function.

The synchrotron-radiation experiments were performed at SPring-8 and Photon Factory. We thank the beamline staff at BL41XU of SPring-8 (Harima, Japan) and NW12 of PF-AR (Tsukuba, Japan) for technical help during data collection.

References

Adachi, H., Niino, A., Murakami, S., Takano, K., Matsumura, H., Kinoshita, T., Warizaya, M., Inoue, T., Mori, Y. & Sasaki, T. (2005). *Jpn. J. Appl. Phys.* **44**, 1365–1366.

Adachi, H., Takano, K., Hosokawa, Y., Inoue, T., Mori, Y., Matsumura, H., Yoshimura, M., Tsunaka, Y., Morikawa, M., Kanaya, S., Masuhara, H., Kai, Y. & Sasaki, T. (2003). *Jpn. J. Appl. Phys.* **42**, L798–L800.

Adachi, H., Takano, K., Yoshimura, M., Mori, Y. & Sasaki, T. (2003). *Jpn. J. Appl. Phys.* **42**, L314–L315.

Alhassid, A., Ben-David, A., Tabachnikov, O., Libster, D., Naveh, E., Zolotnitsky, G., Shoham, Y. & Shoham, G. (2009). *Biochem. J.* **422**, 73–82.

Bacic, A., Harris, P. J. & Stone, B. A. (1988). *The Biochemistry of Plants*, Vol. 14, *Carbohydrates*, edited by J. Preiss, pp. 297–371. London: Academic Press.
Cantarel, B. L., Coutinho, P. M., Rancurel, C., Bernard, T., Lombard, V. & Henrissat, B. (2009). *Nucleic Acids Res.* **37**, D233–D238.
Carapito, R., Imberty, A., Jeltsch, J. M., Byrns, S. C., Tam, P. H., Lowary, T. L., Varrot, A. & Phalip, V. (2009). *J. Biol. Chem.* **284**, 12285–12296.
Cleland, W. W. & Kreevoy, M. M. (1994). *Science*, **264**, 1887–1890.
DeLano, W. L. (2002). *PyMOL.* DeLano Scientific, San Carlos, California, USA.
Fülöp, V. & Jones, D. T. (1999). *Curr. Opin. Struct. Biol.* **9**, 715–721.
Henrissat, B. (1998). *Biochem. Soc. Trans.* **26**, 153–156.
Jawad, Z. & Paoli, M. (2002). *Structure*, **10**, 447–454.
Jones, L., Milne, J. L., Ashford, D. & McQueen-Mason, S. J. (2003). *Proc. Natl Acad. Sci. USA*, **100**, 11783–11788.
Kaneko, S., Arimoto, M., Ohba, M., Kobayashi, H., Ishii, T. & Kusakabe, I. (1998). *Appl. Environ. Microbiol.* **64**, 4021–4027.
Laskowski, R. A., MacArthur, M. W., Moss, D. S. & Thornton, J. M. (1993). *J. Appl. Cryst.* **26**, 283–291.
McRee, D. E. (1999). *J. Struct. Biol.* **125**, 156–165.
Morris, R. J., Perrakis, A. & Lamzin, V. S. (2002). *Acta Cryst.* D**58**, 968–975.
Nelson, N. (1944). *J. Biol. Chem.* **153**, 375–380.
Numan, M. T. & Bhosle, N. B. (2006). *J. Ind. Microbiol. Biotechnol.* **33**, 247–260.
Nurizzo, D., Turkenburg, J. P., Charnock, S. J., Roberts, S. M., Dodson, E. J., McKie, V. A., Taylor, E. J., Gilbert, H. J. & Davies, G. J. (2002). *Nature Struct. Biol.* **9**, 665–668.
Otwinowski, Z. & Minor, W. (1997). *Methods Enzymol.* **276**, 307–326.
Proctor, M. R., Taylor, E. J., Nurizzo, D., Turkenburg, J. P., Lloyd, R. M., Vardakou, M., Davies, G. J. & Gilbert, H. J. (2005). *Proc. Natl Acad. Sci. USA*, **102**, 2697–2702.
Sakamoto, T. (2006). *J. Appl. Glycosci.* **53**, 115–122.
Sakamoto, T., Fujita, T. & Kawasaki, H. (2004). *Biochem. Biophys. Acta*, **1674**, 85–90.
Sakamoto, T., Ihara, H., Shibano, A., Kasai, N., Inui, H. & Kawasaki, H. (2004). *FEBS Lett.* **560**, 199–204.
Sakamoto, T. & Thibault, J. F. (2001). *Appl. Environ. Microbiol.* **67**, 3319–3321.
Schiøtt, B., Iversen, B. B., Madsen, G. K., Larsen, F. K. & Bruice, T. C. (1998). *Proc. Natl Acad. Sci. USA*, **95**, 12799–12802.
Seri, K., Sanai, K., Matsuo, N., Kawakubo, K., Xue, C. & Inoue, S. (1996). *Metabolism*, **45**, 1368–1374.
Sheldrick, G. M. (2008). *Acta Cryst.* A**64**, 112–122.
Somogyi, M. (1952). *J. Biol. Chem.* **195**, 19–23.
Terwilliger, T. C. (2000). *Acta Cryst.* D**56**, 965–972.
Terwilliger, T. C. & Berendzen, J. (1999). *Acta Cryst.* D**55**, 849–861.
Willats, W. G., Steele-King, C. G., Marcus, S. E. & Knox, J. P. (1999). *Plant J.* **20**, 619–628.
Winn, M. D., Murshudov, G. N. & Papiz, M. Z. (2003). *Methods Enzymol.* **374**, 300–321.
Yamaguchi, A., Tada, T., Wada, K., Nakaniwa, T., Kitatani, T., Sogabe, Y., Takao, M., Sakai, T. & Nishimura, K. (2005). *J. Biochem.* **137**, 587–592.